Version TOL/2

EGT3
ENGINEERING TRIPOS PART IIB

Tuesday April 23, 2024 14.00 to 15.40

Module 4G7

CONTROL & COMPUTATION IN LIVING SYSTEMS

*Answer **both** questions in section A. Answer **one** question in section B.*

All questions carry the same number of marks.

*The **approximate** percentage of marks allocated to each part of a question is indicated in the right margin.*

*Write your candidate number **not** your name on the cover sheet.*

STATIONERY REQUIREMENTS
Single-sided script paper

SPECIAL REQUIREMENTS TO BE SUPPLIED FOR THIS EXAM
CUED approved calculator allowed
Attachment 1: 2011 Science paper for Question 3 (5 pages)
Attachment 2: 2000 Nature paper for Question 4 (5 pages)
Engineering Data Book

10 minutes reading time is allowed for this paper at the start of the exam.

You may not start to read the questions printed on the subsequent pages of this question paper until instructed to do so.

You may not remove any stationery from the Examination Room.

SECTION A

Answer **both** questions.

1 (a) Provide two reasons why membrane ion transport is important for sustaining life in non-excitable cells. [10%]

(b) The Hodgkin-Huxley model of the squid giant axon can be written as follows:

$$\dot{v} = -g_{Na}m^3h(v - e_{Na}) - g_K n^4(v - e_K) - g_L(v - e_L) + I_{inp} \quad (1)$$

$$\tau_m(v)\dot{m} = m_\infty(v) - m \quad (2)$$

$$\tau_h(v)\dot{h} = h_\infty(v) - h \quad (3)$$

$$\tau_n(v)\dot{n} = n_\infty(v) - n \quad (4)$$

where v denotes membrane potential, I_{inp} is injected current and the g_x, e_x are, respectively, conductance densities (normalised to membrane capacitance) and reversal potentials (in mV) of the different ionic currents, Na (sodium), K (potassium) and L (leak). The functions $x_\infty(v)$ and $\tau_x(v)$ are plotted in Fig. 1.

(i) Explain the significance and biological interpretation of the variables m, h and n. [5%]

(ii) Sketch the evolution of the membrane potential and of m, h and n in response to continuous current injection of sufficient amplitude to elicit repetitive action potentials. [10%]

(iii) Sketch the response of the sodium and potassium conductance to a depolarising voltage step starting from an initial value close to the equilibrium potential of the membrane. [10%]

(iv) Referring to your sketch in (iii), plot the "early" and "late" components of the membrane current as a function of depolarising voltage steps from an initial value of -80 mV to values in the range $[-80, 50]$ mV. [15%]

(v) Use your sketches in parts (ii-iv) to explain the form of the Fitzhugh-Nagumo model:

$$\dot{V} = 10(-V^3/3 + V - R + I_{inp}) \quad (5)$$

$$\dot{R} = 0.8(1.25V - R + 1.5) \quad (6)$$

[20%]

(cont.

(c) Consider an *integrate and fire* model of a neuron in which membrane potential evolves according to:

$$\begin{cases} C\dot{V} = g(V_0 - V) & \text{if } V < V_{\text{thr}} \\ V_{\text{reset}} \hookleftarrow V & \text{otherwise} \end{cases}$$

(i) Suppose the membrane potential is subjected to a train of impulses separated by a time interval, T, each depolarising the membrane potential by an amplitude, A. Derive a condition on A and T for the membrane to reach threshold. [20%]

(ii) Suppose instead that the membrane is subjected to constant depolarising current. Sketch the firing frequency as a function of current amplitude. How does this relationship differ from that of the Fizhugh-Nagumo model in question 1b(v)? [10%]

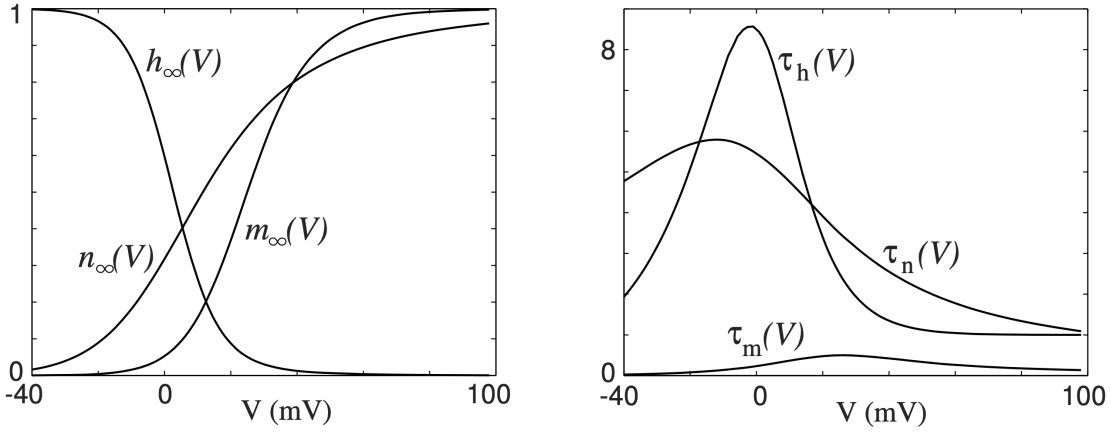

Fig. 1: plots of the voltage-dependent functions for the Hodgkin Huxley model in Question 1(b). Units of the $\tau_x(V)$ are ms.

2 (a) Consider a discrete time model of diffusion as a 1D random walk, in which a particle's position, x_n, randomly increments position by $\pm d$ in each timestep, n.

(i) Derive expressions for the expected displacement, $\mathbb{E}(x_n)$, and expected squared displacement, $\mathbb{E}(x_n^2)$, in the general case where there may be a bias between positive and negative increments. You may state without proof formulae for the mean and variance of the Binomial distribution. [15%]

(ii) Now suppose the probability of an increment of $-d, +d$ is equal and independent for each component. Derive an expression for $\mathbb{E}(x_n^T x_n)$ in the case where $x \in \mathbb{R}_{\mathbb{N}}$ has N components. [15%]

(iii) Discuss the implications of your answer to (i) for the speed of chemical signalling within cells of different sizes. [10%]

(b) In three dimensions the diffusion equation is:

$$\frac{\partial f}{\partial t} = D\nabla^2 f; \qquad \text{where } \nabla^2 f = \frac{\partial^2 f}{\partial x_1^2} + \frac{\partial^2 f}{\partial x_2^2} + \frac{\partial^2 f}{\partial x_3^2}.$$

(i) Assuming a radially symmetrical solution about the origin, rewrite the three dimensional diffusion equation in terms of r, with $r^2 = x_1^2 + x_2^2 + x_3^2$. [30%]

(ii) By writing the radially symmetric solution in the form $f(r,t) = \frac{\theta(r,t)}{r}$, show that θ obeys a one dimensional diffusion equation. [30%]

SECTION B

Answer **one** question.

3 Refer to the attached paper by Couzin et al (2011) Science.

(a) Summarise the aim, approach, findings and motivation of the paper in no more than 500 words. Provide an interpretation of the results and comment on any limitations of the study. You may use diagrams if you wish. [60%]

(b) What is meant by a *bifurcation* in the context of a dynamical system? Describe the saddle-node and pitchfork bifurcations, and any relevance they may have to Figure 2B of Couzin et al. [40%]

4 Refer to the attached paper by Elowitz & Leibler (2000) Nature.

(a) Summarise the aim, approach, findings and motivation of the paper in no more than 500 words. Provide an interpretation of the results and comment on any limitations of the study. You may use diagrams if you wish. [60%]

(b) Consider a simpler version of the system modelled in Box 1 of Elowitz & Leibler with only one mRNA/protein species:

$$\dot{m} = -m + \frac{\alpha}{1 + p^n} + \alpha_0$$
$$\dot{p} = -\beta(p - m)$$

where the symbols are defined in the paper. Would this simpler system be capable of generating oscillations, theoretically? What factors might violate your prediction if the system were experimentally implemented in a living cell? [40%]

END OF PAPER

THIS PAGE IS BLANK

Uninformed Individuals Promote Democratic Consensus in Animal Groups

Iain D. Couzin,[1]* Christos C. Ioannou,[1]† Güven Demirel,[2] Thilo Gross,[2]‡ Colin J. Torney,[1] Andrew Hartnett,[1] Larissa Conradt,[3]§ Simon A. Levin,[1] Naomi E. Leonard[4]

Conflicting interests among group members are common when making collective decisions, yet failure to achieve consensus can be costly. Under these circumstances individuals may be susceptible to manipulation by a strongly opinionated, or extremist, minority. It has previously been argued, for humans and animals, that social groups containing individuals who are uninformed, or exhibit weak preferences, are particularly vulnerable to such manipulative agents. Here, we use theory and experiment to demonstrate that, for a wide range of conditions, a strongly opinionated minority can dictate group choice, but the presence of uninformed individuals spontaneously inhibits this process, returning control to the numerical majority. Our results emphasize the role of uninformed individuals in achieving democratic consensus amid internal group conflict and informational constraints.

Social organisms must often achieve a consensus to obtain the benefits of group living and to avoid the costs of indecision (*1*–*12*). In some societies, notably those of eusocial insects, making consensus decisions is often a unitary, conflict-free process because the close relatedness among individuals means that they typically share preferences (*11*). However, in other social animals, such as schooling fish, flocking birds, herding ungulates, and humans, individual group members may be of low relatedness; thus, self-interest can play an important role in group decisions. Reaching a consensus decision, therefore, frequently depends on individuals resolving complex conflicts of interest (*1*–*11*, *13*, *14*).

There are several means of achieving group consensus. In some cases, decisions made by one or only a small proportion of the group dictate the behavior of the entire group (*4*–*6*, *13*, *14*). Therefore, a minority, or even a single individual, has the potential to control or exploit the majority, achieving substantial gains at the expense of other group members (*1*–*6*, *9*, *10*, *14*). In contrast, consensus can also be reached through democratic means, with fair representation and an outcome determined by a plurality. Democratic decisions tend to be more moderate, minimizing group consensus costs, particularly in large animal groups (*3*). However, in the absence of established procedures such as voting (*8*), it is unclear how equal representation is enforced.

Consequently, for both human societies (*1*, *2*, *6*, *9*, *10*, *14*) and group-living animals (*6*, *13*), it has been argued that group decisions can be subject to manipulation by a self-interested and opinionated minority. In particular, previous work suggests that groups containing individuals who are uninformed, or naïve, about the decision being made are particularly vulnerable to such manipulation (*2*, *9*, *10*, *13*). Under this view, uninformed individuals destabilize the capacity for collective intelligence in groups (*10*, *14*), with poorly informed individuals potentially facilitating the establishment of extremist opinions in populations (*9*, *14*).

Here, we address the question of whether and, if so, under which conditions a self-interested and strongly opinionated minority can exert its influence on group movement decisions. We show that uninformed individuals (defined as those who lack a preference or are uninformed about the features on which the collective decision is being made) play a central role in achieving democratic consensus.

We use a spatially explicit computational model of animal groups (*15*) that makes minimal assumptions regarding the capabilities of individual group members; they are assumed to avoid collisions with others and otherwise exhibit the capacity to be attracted toward, and to align direction of travel with, near neighbors (*5*, *16*). We investigate the case of consensus decision-making regarding a choice to move to one of two discrete targets in space (thus, the options are mutually exclusive).

The direction and strength of an individual's preference are encoded in a vector term $\vec{\omega}$ (directed toward the individual's preferred target). Higher scalar values of ω (equivalent to the length of the $\vec{\omega}$ vector, $\omega \equiv |\vec{\omega}|$) represent a greater conviction in, or strength of, individual preference to move in the direction of the target and, thus, also represent greater intransigence to social influence (*5*).We explore the case where there are two subpopulations within the group—N_1 and N_2, respectively—that have different preferred targets. Because we are interested in determining whether a minority can exploit a majority, we set $N_1 > N_2$ for the simulation. The strengths of the preference of the numerical majority and minority are represented by their respective ω values, ω_1 and ω_2. See (*15*) for details.

If the strength of the majority preference (ω_1) is equal to or stronger than the minority preference (ω_2), the group has a high probability of reaching the majority-preferred target (Fig. 1A) (*5*). Yet increasing ω_2 (beyond ω_1) can result

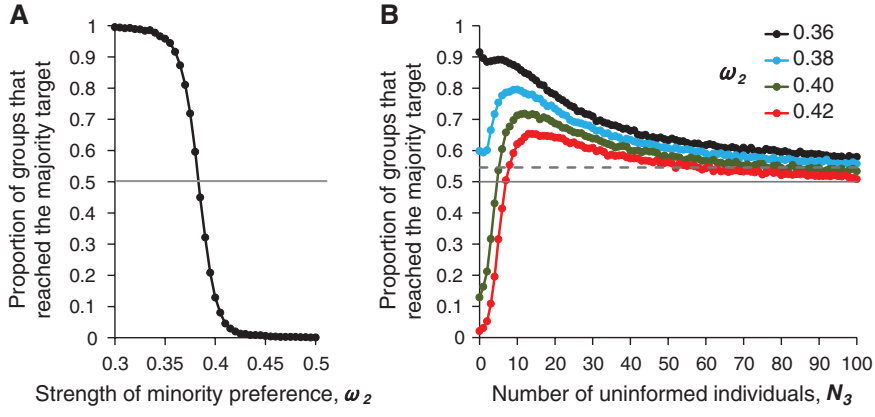

Fig. 1. Spatial simulation of consensus decision-making in which individuals' preferred direction, weighted by their respective ω (see main text), is directed toward their preferred target. (**A**) $\omega_1 = 0.3$. All individuals are informed with majority $N_1 = 6$ and minority $N_2 = 5$. As the minority increases its preference strength, ω_2, it increasingly controls group motion. (**B**) In the presence of sufficient uninformed individuals, the minority can no longer exploit the majority by increasing ω_2 (see fig. S2 for other values of N_1 and N_2). The ratio of the majority to all informed, $N_1/(N_1 + N_2)$, is shown as a horizontal gray dashed line. The proportion reaching the majority target is calculated as the number of times (from 20,000 replicates) the majority-preferred target is reached divided by the number of times a (minority or majority) target was reached (i.e., only consensus decisions were evaluated; splitting was infrequent; see fig. S5). $\omega_1 = 0.3$. See (*15*) for details.

[1]Department of Ecology and Evolutionary Biology, Princeton University, Princeton, NJ 08544, USA. [2]Max Planck Institute for Physics of Complex Systems, Nöthnitzer Strasse, 01187 Dresden, Germany. [3]School of Life Sciences, John Maynard Smith Building, University of Sussex, Falmer, Brighton BN1 9QG, UK. [4]Department of Mechanical and Aerospace Engineering, Princeton University, Princeton, NJ 08544, USA.

*To whom correspondence should be addressed. E-mail: icouzin@princeton.edu

†Present address: School of Biological Sciences, University of Bristol, Woodland Road, Bristol BS8 1UG, UK.

‡Present address: Merchant Venturers School of Engineering, University of Bristol, Bristol BS8 1UB, UK.

§Present address: Department of Zoology, Downing Street, University of Cambridge, Cambridge CB2 3EU, UK.

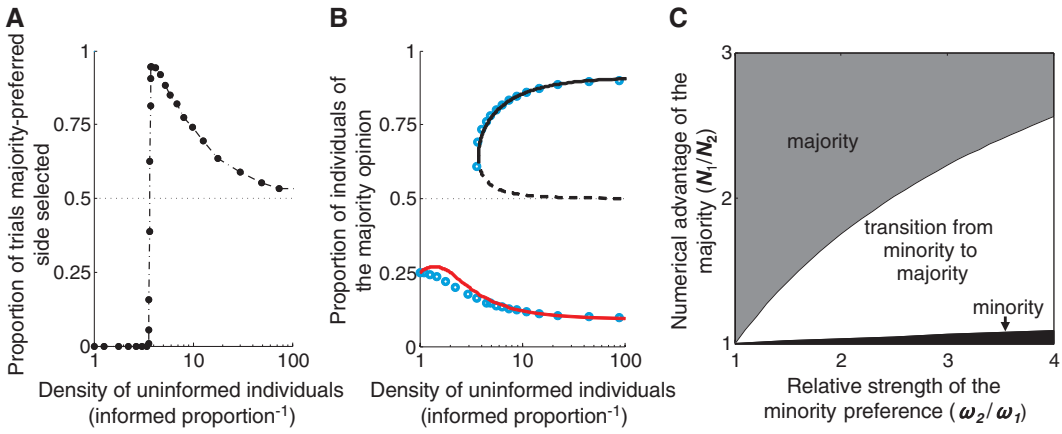

Fig. 2. The adaptive-network model (*17*, *21*–*23*) provides an analytically tractable analog to the spatially explicit model. (**A**) Network simulations show qualitative agreement with the spatial model. (**B**) An analytical approximation of the model reveals the dynamical cause of this transition. For low densities of uninformed individuals, the minority-controlled state (red line) is the only stable attractor. As the proportion of uninformed individuals increases, the system undergoes a saddle-node bifurcation resulting in a stable majority-controlled state (solid black line) and an unstable undecided state (dashed black line). Simulations (blue circles) closely match analytical approximations. (**C**) In this phase diagram, we see the outcome of opinion formation as a function of the ratio of the majority to minority subpopulation (N_1/N_2) and the relative strength of the minority preference (equivalent to ω_2/ω_1) measured in terms of the ratio of switching rates [see (*15*) for details]. The white region of the phase diagram represents the region in which this saddle-node bifurcation results in a transition from minority to majority control when sufficient uninformed individuals are present. The regions denoted "majority" and "minority" represent parameter space where the N_1 or N_2 preferences, respectively, are adopted regardless of the number of uninformed individuals ($N_3 \in [0,\infty]$).

in the minority gaining control and eventually dictating group outcome (Fig. 1A and fig. S1). If some individuals do not have relevant prior information or are only weakly biased, however, as is likely in many animal groups (*5*, *6*, *13*), then groups can be considered to have a third subpopulation of N_3 individuals with $\omega_3 \approx 0$. Now when ω_2 is in the range where the minority dictates the group outcome for $N_3 = 0$, adding uninformed individuals tends to return control spontaneously to the numerical majority (Fig. 1B) ($\omega_2 = 0.4, 0.42$). As N_3 increases, this effect reaches a maximum and then begins to slowly diminish. Eventually, noise dominates and uninformed individuals neither amplify a weak numerical majority nor lend substantial support to the minority.

To determine whether these results can be generalized, we develop reduced, analytically tractable versions of the above model. The first, modified from (*17*), represents individuals as nodes on a network with interindividual communication represented by a dynamically changing edge topology. A second (increasingly minimalist) approach considers a convention game of self-reinforcing normative opinion dynamics (*18*). These simplified models are nonspatial and consider discrete (binary) opinions, yet incorporate key features of the spatial model: (i) Individuals adopt, probabilistically, the opinion they perceive to be that of the local majority (this results in positive feedback reinforcing the predominant opinion and, consequently, rapid nonlinear transitions from disordered to ordered consensus states). (ii) The strength of individual preference manifests as intransigence during interactions with others.

These models capture the same qualitative collective features as the spatial model (*15*). Figure 2A shows the presence of a sharp transition from a minority- to majority-controlled outcome in the network model as the density of uninformed individuals is increased. Analysis reveals the dynamical nature of this transition (Fig. 2B) (*15*), as well as the large region of parameter space in which a minority-preferred outcome switches to a majority-preferred outcome if sufficient uninformed individuals are present (white region in Fig. 2C).

In all models, an entrenched minority is capable of exerting substantial influence by biasing the perceived consensus. Because they exhibit little intransigence or intrinsic bias, however, uninformed individuals will lend support to, and tend to amplify, a numerical advantage (even a slight one). If sufficiently numerous, they reduce the effect of intransigence and inhibit the capacity for the minority to take hold, thus returning control to the numerical majority. Consequently, even a small change in the number of uninformed individuals can dramatically alter the outcome of consensus decisions (Figs. 1B and 2A and figs. S7A and S8) (*15*). We emphasize that this process will tend to inhibit any strong minority preference, regardless of the intrinsic quality or value of that view. We conjecture that this phenomenon may be found in seemingly disparate systems that share those common features outlined above (*15*).

Our theoretical studies make a primary testable prediction: Uninformed individuals should inhibit the influence of a strongly opinionated minority, returning control to the numerical majority. To test this prediction, we conducted experiments with golden shiners (*Notemigonus crysoleucas*) (Fig. 3A, inset), a strongly schooling species of freshwater fish (*19*). We trained two subpopulations of individuals (representing either N_1 or N_2) to have preferences to move from a starting location toward either a blue target or a yellow target (Fig. 3B and figs. S3 and S4) (*15*). Under our experimental conditions, shiners exhibited a spontaneous preexisting bias toward the yellow target (*15*, *20*), evident in both training (figs. S10 and S11) and testing (see results, below). Consequently, we did not need to

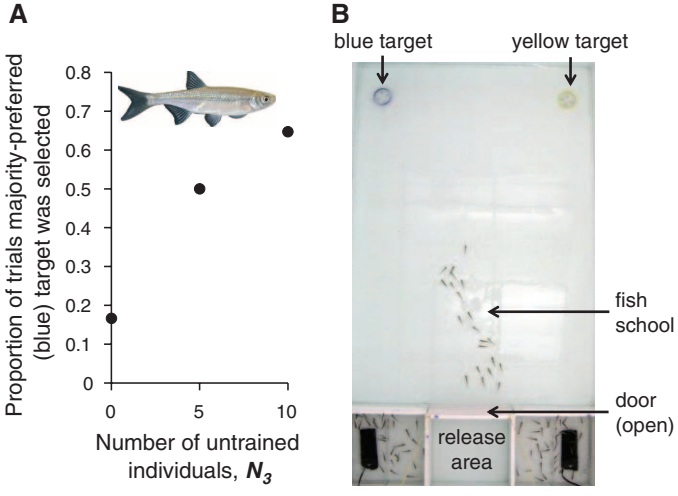

Fig. 3. Experiments with schooling fish demonstrate support for our hypothesis. (**A**) When the minority ($N_2 = 5$) are trained to the intrinsically preferred (yellow) target, inclusion of untrained individuals returns control from a dominating minority to the numerical majority (18 replicates per data point). (Inset) A golden shiner is shown. (**B**) Image from an experimental video with $N_1 = 6$, $N_2 = 5$, and $N_3 = 10$. See fig. S3 and (*15*) for further details.

employ different training regimes to create a difference in the strength of preference between our two trained subpopulations (*15*). A third (N_3) subpopulation was left untrained.

Because our theoretical predictions do not depend on the absolute number of N_1 individuals (fig. S2), and due to the time-consuming nature of training and constraints related to obtaining enough fish for replication, we set $N_1 = 6$ and $N_2 = 5$ fish (as in Fig. 1). Our simulations also predict a large effect for a relatively small number of naïve individuals (Fig. 1B); thus, we set $N_3 = 0$, 5, or 10. When N_2 fish are trained to the yellow (biased) target and all individuals exhibit a preference ($N_3 = 0$), the minority N_2 dictates the consensus achieved, even though the fish trained to the blue target are more numerous. However, when untrained individuals are present, they increasingly return control to the numerical majority N_1 (Fig. 3A) [generalized linear model (GLM); likelihood ratio test $(LRT)_{1,52} = 5.60$, $P = 0.018$]. A snapshot from a trial is shown in Fig. 3B. We also performed experiments in which individuals with the stronger preference were also in the numerical majority (N_1 trained to the yellow target). As expected (*15*), the majority was more likely to win (72% of trials overall), and the presence of uninformed individuals had no effect (12, 16, and 11 of 18 replicates for $N_3 = 0$, 5, and 10, respectively; GLM; $LRT_{1,52} = 0.14$, $P = 0.71$).

Our work provides evidence that uninformed individuals play an important role in consensus decision-making: By enforcing equal representation of preferences in a group, they promote a democratic outcome. This provides a new understanding of how informational status influences consensus decisions and why consensus decision-making may be so widespread in nature (*4*). Furthermore, these results suggest a principle that may extend to self-organized decisions among human agents.

References and Notes

1. K. Arrow, *Social Choices and Individual Values* (Yale Univ. Press, New Haven, CT, ed. 2, 1963).
2. J. M. Buchanan, G. Tullock, *The Calculus of Consent: Logical Foundations of Constitutional Democracy* (Liberty Fund, Indianapolis, IN, 1958).
3. L. Conradt, T. J. Roper, *Nature* **421**, 155 (2003).
4. L. Conradt, T. J. Roper, *Trends Ecol. Evol.* **20**, 449 (2005).
5. I. D. Couzin, J. Krause, N. R. Franks, S. A. Levin, *Nature* **433**, 513 (2005).
6. A. J. King, D. D. P. Johnson, M. Van Vugt, *Curr. Biol.* **19**, R911 (2009).
7. J. Krause, G. D. Ruxton, *Living in Groups* (Oxford Univ. Press, Oxford, 2002).
8. J. Mansbridge, *Beyond Adversary Democracy* (The Univ. of Chicago Press, Chicago, 1983).
9. M. Olson Jr., *The Logic of Collective Action: Public Goods and the Theory of Groups* (Harvard Univ. Press, Cambridge, MA, 1971).
10. W. Riker, *Liberalism Against Populism: A Confrontation Between the Theory of Democracy and the Theory of Social Choice* (W. H. Freeman, San Francisco, 1982).
11. T. D. Seeley, *Honeybee Democracy* (Princeton Univ. Press, Princeton, NJ, 2010).
12. A. J. Ward, J. E. Herbert-Read, D. J. T. Sumpter, J. Krause, *Proc. Natl. Acad. Sci. U.S.A.* **108**, 2312 (2011).
13. L. Conradt, J. Krause, I. D. Couzin, T. J. Roper, *Am. Nat.* **173**, 304 (2009).
14. S. Issacharoff, *Int. J. Const. Law* **6**, 231 (2008).
15. Materials and methods are available as supporting material on *Science* Online.
16. Y. Katz, K. Tunstrøm, C. C. Ioannou, C. Huepe, I. D. Couzin, *Proc. Natl. Acad. Sci. U.S.A.* **108**, 18720 (2011).
17. C. Huepe, G. Zschaler, A.-L. Do, T. Gross, *New J. Phys.* **13**, 073022 (2011).
18. H. P. Young, *Individual Strategy and Social Structure: An Evolutionary Theory of Institutions* (Princeton Univ. Press, Princeton, NJ, 1998).
19. S. G. Reebs, *Anim. Behav.* **59**, 403 (2000).
20. R. Spence, R. Smith, *Ethology* **114**, 582 (2008).
21. P. Holme, M. E. J. Newman, *Phys. Rev. E.* **74**, 056108 (2006).
22. F. Vazquez, V. M. Eguíluz, M. San Miguel, *Phys. Rev. Lett.* **100**, 108702 (2008).
23. D. H. Zanette, S. Gil, *Physica D* **224**, 156 (2006).

Acknowledgments: We thank H. Li, L. Petzold, J. Moehlis, A. Kolpas, Y. Katz, and A. Kao for help with CUDA and the Couzin lab for discussions. This work was supported by NSF grant PHY-0848755, the Searle Scholars Program, Office of Naval Research grant N00014-09-1-1074, Defense Advanced Research Projects Agency grant HR0011-09-1-0055, and The Royal Society. I.D.C. devised the study and performed and analyzed the spatial simulations, C.C.I. performed and analyzed the fish experiments, and G.D. and T.G. performed the adaptive networks model and C.J.T. the convention model. All authors participated in some aspects of model formulation and analysis. I.D.C. wrote the paper with input from all authors. Data and code freely available at http://icouzin.princeton.edu/uninformed-individuals-promote-democratic-consensus-in-animal-groups/.

Supporting Online Material

www.sciencemag.org/cgi/content/full/334/6062/1578/DC1
Materials and Methods
SOM Text
Figs. S1 to S12
Table S1
References (*24*–*27*)

24 June 2011; accepted 3 November 2011
10.1126/science.1210280

Western blotting

Ribosomal complexes assembled and purified as described above were TCA-precipitated. Proteins were resolved on 12% polyacrylamide gel, transferred to nitrocellulose membrane and probed for eIF1 and eIF5B using T7-tag antibodies (Novagen) and for eIF2α and eIF3 (p170) using specific antibodies.

Received 13 September; accepted 16 November 1999.

1. Merrick, W. C. Mechanism and regulation of eukaryotic protein synthesis. *Microbiol. Rev.* **56,** 291–315 (1992).
2. Pestova, T. V., Borukhov, S. I. & Hellen, C. U. T. Eukaryotic ribosomes require initiation factors 1 and 1A to locate initiation codons. *Nature* **394,** 854–859 (1998).
3. Chakrabarti, A. & Maitra, U. Functions of eukaryotic initiation factor 5 in the formation of an 80S ribosomal polypeptide chain initiation complex. *J. Biol. Chem.* **266,** 14039–14045 (1991).
4. Das, K., Chesevich, J. & Maitra, U. Molecular cloning and expression of cDNA for mammalian translation initiation factor 5. *Proc. Natl Acad. Sci. USA* **90,** 3058–3062 (1993).
5. Huang, H.-K., Yoon, H., Hannig, E. M. & Donahue, T. F. GTP hydrolysis controls stringent selection of the AUG start codon during translation initiation in *Saccharomyces cerevisiae*. *Genes Dev.* **11,** 2396–2413 (1997).
6. Choi, S. K., Lee, J. H., Zoll, W. L., Merrick, W. C. & Dever, T. E. Promotion of Met-tRNA^{Met} binding to ribosomes by yIF2, a bacterial IF2 homolog in yeast. *Science* **280,** 1757–1760 (1998).
7. Lee, J. H., Choi, S. K., Roll-Mecak, A., Burley, S. K. & Dever, T. E. Universal conservation in translation initiation revealed by human and archaeal homologs of bacterial translation factor IF2. *Proc. Natl Acad. Sci. USA* **96,** 4342–4347 (1999).
8. Sacerdot, C., Dessen, P., Hershey, J. W. B., Plumbridge, J. A. & Grunberg-Manago, M. Sequence of the initiation factor IF2 gene; unusual protein features and homologies with elongation factors. *Proc. Natl Acad. Sci. USA* **81,** 7787–7791 (1984).
9. Kolakofsky, D., Dewey, K. F., Hershey, J. W. B. & Thach, R. E. Guanosine 5′-triphosphatase activity of initiation factor f2. *Proc. Natl Acad. Sci. USA* **61,** 1066–1070 (1968).
10. Godefroy-Colburn, T. *et al*. Light-scattering studies showing the effect of initiation factors on the reversible dissociation of *Escherichia coli* ribosomes. *J. Mol. Biol.* **94,** 461–478 (1975).
11. Luchin, S. *et al*. *In vitro* study of two dominant inhibitory GTPase mutants of *Escherichia coli* translation initiation factor IF2. Direct evidence that GTP hydrolysis is necessary for factor recycling. *J. Biol. Chem.* **274,** 6074–6079 (1999).
12. Lockwood, A. H., Sarkar, P. & Maitra, U. Release of polypeptide chain initiation factor IF-2 during initiation complex formation. *Proc. Natl Acad. Sci. USA* **69,** 3602–3605 (1972).
13. Merrick, W. C., Kemper, W. M. & Anderson, W. F. Purification and characterization of homogenous initiation factor M2A from rabbit reticulocytes. *J. Biol. Chem.* **250,** 5556–5562 (1975).
14. Trachsel, H., Emi, B., Schreier, M. H. & Staehelin, T. Initiation of mammalian protein synthesis. II. The assembly of the initiation complex with purified initiation factors. *J. Mol. Biol.* **116,** 755–767 (1977).
15. Benne, R., Brown-Luedi, M. L. & Hershey, J. W. B. Purification and characterization of protein synthesis initiation factors eIF-1, eIF-4C, eIF-4D, and eIF-5 from rabbit reticulocytes. *J. Biol. Chem.* **253,** 3070–3077 (1978).
16. Peterson, D. T., Safer, B. & Merrick, W. C. Role of eukaryotic initiation factor 5 in the formation of 80S initiation complexes. *J. Biol. Chem.* **254,** 7730–7735 (1979).
17. Pestova, T. V., Shatsky, I. N., Fletcher, S. P., Jackson, R. J. & Hellen, C. U. T. A prokaryotic-like mode of binding of cytoplasmic eukaryotic ribosomes to the initiation codon during internal initiation of translation of Hepatitis C and Classical Swine fever virus RNAs. *Genes Dev.* **12,** 67–83 (1998).

Acknowledgements

We thank W. Merrick for discussions, D. Etchison and R. Schneider for antibodies, and L. Siconolfi-Baez for sequencing eIF5B. These studies were supported by grants from the NIH to C.U.T.H. and T.V.P.

Correspondence and requests for materials should be addressed to T.V.P. (e-mail: tpestova@netmail.hscbklyn.edu).

A synthetic oscillatory network of transcriptional regulators

Michael B. Elowitz & Stanislas Leibler

Departments of Molecular Biology and Physics, Princeton University, Princeton, New Jersey 08544, USA

Networks of interacting biomolecules carry out many essential functions in living cells[1], but the 'design principles' underlying the functioning of such intracellular networks remain poorly understood, despite intensive efforts including quantitative analysis of relatively simple systems[2]. Here we present a complementary approach to this problem: the design and construction of a synthetic network to implement a particular function. We used three transcriptional repressor systems that are not part of any natural biological clock[3–5] to build an oscillating network, termed the repressilator, in *Escherichia coli*. The network periodically induces the synthesis of green fluorescent protein as a readout of its state in individual cells. The resulting oscillations, with typical periods of hours, are slower than the cell-division cycle, so the state of the oscillator has to be transmitted from generation to generation. This artificial clock displays noisy behaviour, possibly because of stochastic fluctuations of its components. Such 'rational network design' may lead both to the engineering of new cellular behaviours and to an improved understanding of naturally occurring networks.

In the network shown in Fig. 1a, the first repressor protein, LacI from *E. coli*, inhibits the transcription of the second repressor gene, *tetR* from the tetracycline-resistance transposon Tn*10*, whose protein product in turn inhibits the expression of a third gene, *cI* from λ phage. Finally, CI inhibits *lacI* expression, completing the cycle. That such a negative feedback loop can lead to temporal oscillations in the concentrations of each of its components can be seen from a simple model of transcriptional regulation, which we used to design the repressilator and study its possible behaviours (Box 1). In this model, the action of the network depends on several factors, including the dependence of transcription rate on repressor concentration, the translation rate, and the decay rates of the protein and messenger RNA. Depending on the values of these parameters, at least two types of solutions are possible: the system may converge toward a stable steady state, or the steady state may become unstable, leading to sustained limit-cycle oscillations (Fig. 1b, c).

We found that oscillations are favoured by strong promoters coupled to efficient ribosome-binding sites, tight transcriptional repression (low 'leakiness'), cooperative repression characteristics, and comparable protein and mRNA decay rates (Box 1, Fig. 1b). A general obstacle to the design of biochemical networks is uncertainty about the values of parameters that characterize the interactions between different components. In our network, estimates of the order of magnitude of the relevant parameters seem to be compatible with the possibility of oscillations. Nevertheless, to increase the chances that the artificial network would function in the oscillatory regime, we made two alterations to natural components. First, to address transcriptional strength and tightness, we used strong, yet tightly repressible hybrid promoters, developed previously, which combine the λ P_L promoter with *lac* and *tet* operator sequences[6]. Second, to bring the effective repressor protein lifetimes closer to that of mRNA (about 2 min, on average, in *E. coli*[7]), we inserted a carboxy-terminal tag, based on the *ssrA* RNA sequence[8], at the 3′ end of each repressor gene. Proteases in *E. coli* recognize this tag and target the attached protein for destruction[9,10]. Such tags have been shown to reduce the half-life of the λ repressor DNA-binding domain from more than 60 min to around 4 min (ref. 8) and diminish the half-life of green fluorescent protein (GFP) to about 30–40 min (ref. 11).

With these considerations in mind, we used standard molecular biology techniques to construct a low-copy plasmid encoding the repressilator and a compatible, higher-copy reporter plasmid containing the tet-repressible promoter $P_L$tetO1 (ref. 6) fused to an intermediate stability variant of *gfp*[11] (Fig. 1a). Because the inducer IPTG interferes with repression by LacI, we expected that a transient pulse of IPTG might be capable of synchronizing a population of repressilator-containing cells. A culture of *E. coli* MC4100 containing the two plasmids and grown in media containing IPTG displayed what appeared to be a single damped oscillation of GFP fluorescence per cell after transfer to media lacking IPTG (results not shown). Because individual cells have no apparent means of maintaining synchronization, we studied the repressilator by isolating single cells under the microscope and monitoring their fluorescence intensity as they grew into small two-dimensional microcolonies consisting of hundreds of progeny cells. In these experiments, total observation time was limited by the colony entering a stationary phase after about 10 hours of growth at

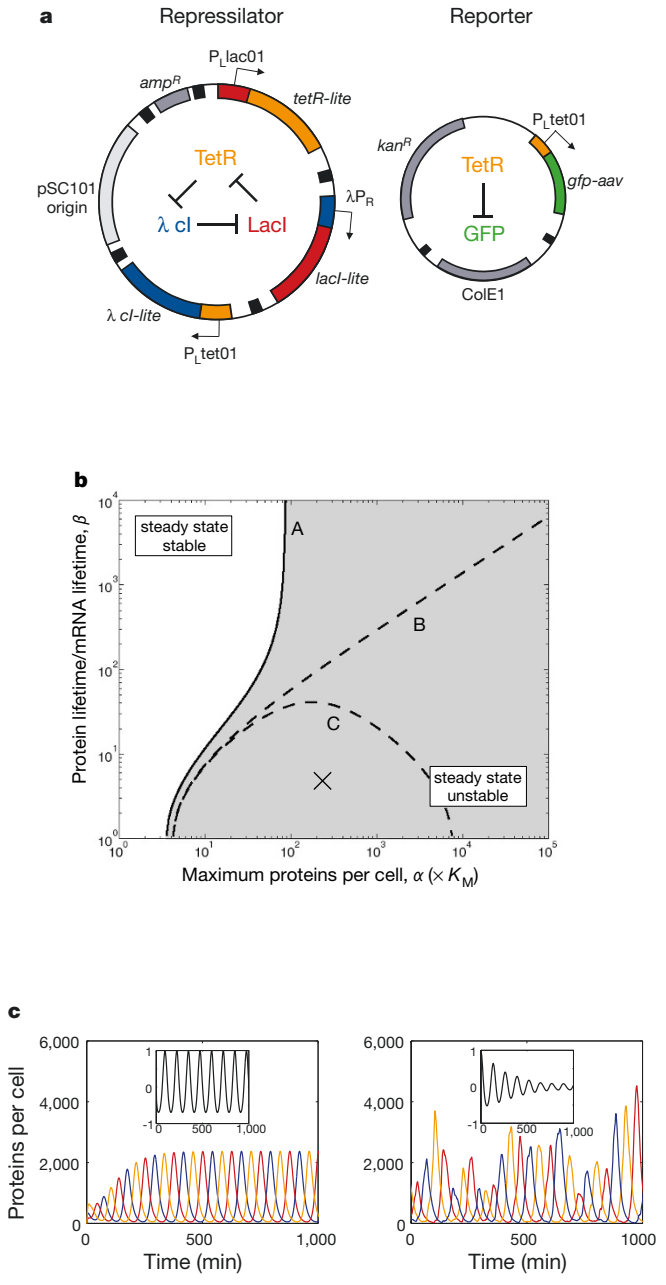

Figure 1 Construction, design and simulation of the repressilator. **a**, The repressilator network. The repressilator is a cyclic negative-feedback loop composed of three repressor genes and their corresponding promoters, as shown schematically in the centre of the left-hand plasmid. It uses $P_L$lacO1 and $P_L$tetO1, which are strong, tightly repressible promoters containing *lac* and *tet* operators, respectively[6], as well as P_R, the right promoter from phage λ (see Methods). The stability of the three repressors is reduced by the presence of destruction tags (denoted '*lite*'). The compatible reporter plasmid (right) expresses an intermediate-stability GFP variant[11] (*gfp-aav*). In both plasmids, transcriptional units are isolated from neighbouring regions by T1 terminators from the *E. coli rrnB* operon (black boxes). **b**, Stability diagram for a continuous symmetric repressilator model (Box 1). The parameter space is divided into two regions in which the steady state is stable (top left) or unstable (bottom right). Curves A, B and C mark the boundaries between the two regions for different parameter values: A, $n = 2.1$, $\alpha_0 = 0$; B, $n = 2$, $\alpha_0 = 0$; C, $n = 2$, $\alpha_0/\alpha = 10^{-3}$. The unstable region (A), which includes unstable regions (B) and (C), is shaded. **c**, Oscillations in the levels of the three repressor proteins, as obtained by numerical integration. Left, a set of typical parameter values, marked by the 'X' in **b**, were used to solve the continuous model. Right, a similar set of parameters was used to solve a stochastic version of the model (Box 1). Colour coding is as in **a**. Insets show the normalized autocorrelation function of the first repressor species.

30 °C. At least 100 individual cell lineages in each of three microcolonies were tracked manually, and their fluorescence intensity was quantified.

The timecourse of the fluorescence of one such cell is shown in Fig. 2. Temporal oscillations (in this case superimposed on an overall increase in fluorescence) occur with a period of around 150 minutes, roughly threefold longer than the typical cell-division time. The amplitude of oscillations is large compared with baseline levels of GFP fluorescence. At least 40% of cells were found to exhibit oscillatory behaviour in each of the three movies, as determined by a Fourier analysis criterion (see Methods). The range of periods, as estimated by the distribution of peak-to-peak intervals, is 160 ± 40 min (mean ± s.d., $n = 63$). After septation, GFP levels in the two sibling cells often remained correlated with one another for long periods of time (Fig. 3a–c). Based on the analysis of 179 septation events in the 3 movies, we measured an average half-time for sibling decorrelation of 95 ± 10 min, which is longer than the typical cell-division times of 50–70 min under these conditions. This indicates that the state of the network is transmitted to the progeny cells, despite a strong noise component. We observed significant variations in the period and amplitude of the oscillator output both from cell to cell (Fig. 3d), and over time in a single cell and its descendants (Fig. 3a–c). In some individuals, periods were omitted or phase delayed in one cell relative to its sibling (Fig. 3a, c).

Recent theoretical work has shown that stochastic effects may be responsible for noisy operation in natural gene-expression networks[12]. Simulations of the repressilator that take into account the stochastic nature of reaction events and discreteness of network components also exhibit significant variability, reducing the correlation time for oscillations from infinity (in the continuous model) to about two periods (Box 1, Fig. 1c, insets). In general, we would like to distinguish such stochastic effects from possible intrinsically complex dynamics (such as intermittence or chaotic behaviour). Further studies are needed to identify and characterize the sources of fluctuations in the repressilator and other designed networks. In particular, longer experiments performed under chemostatic conditions should enable more complete statistical characterization of

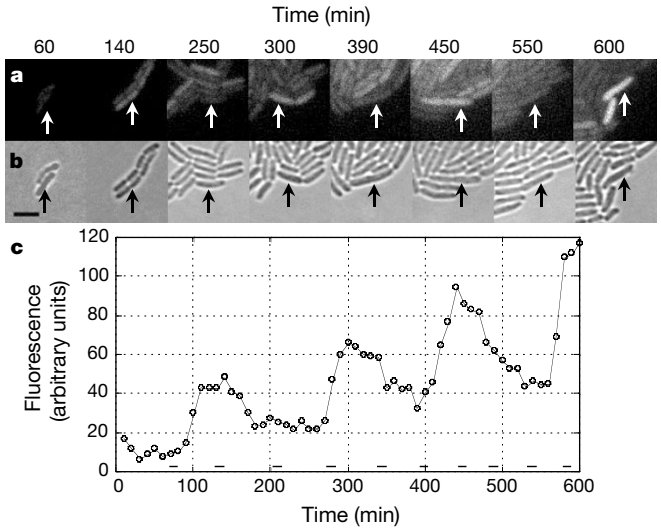

Figure 2 Repressilation in living bacteria. **a**, **b**, The growth and timecourse of GFP expression for a single cell of *E. coli* host strain MC4100 containing the repressilator plasmids (Fig. 1a). Snapshots of a growing microcolony were taken periodically both in fluorescence (**a**) and bright-field (**b**). **c**, The pictures in **a** and **b** correspond to peaks and troughs in the timecourse of GFP fluorescence density of the selected cell. Scale bar, 4 μm. Bars at the bottom of **c** indicate the timing of septation events, as estimated from bright-field images.

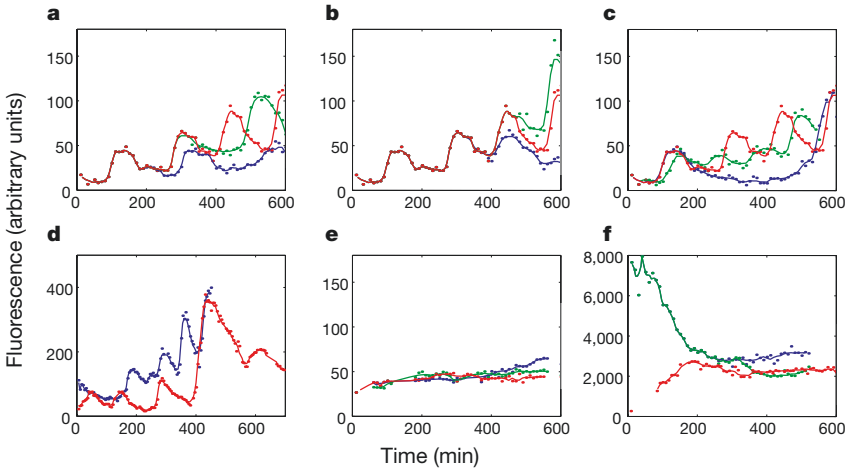

Figure 3 Examples of oscillatory behaviour and of negative controls. **a**–**c**, Comparison of the repressilator dynamics exhibited by sibling cells. In each case, the fluorescence timecourse of the cell depicted in Fig. 2 is redrawn in red as a reference, and two of its siblings are shown in blue and green. **a**, Siblings exhibiting post-septation phase delays relative to the reference cell. **b**, Examples where phase is approximately maintained but amplitude varies significantly after division. **c**, Examples of reduced period (green) and long delay (blue). **d**, Two other examples of oscillatory cells from data obtained in different experiments, under conditions similar to those of **a**–**c**. There is a large variability in period and amplitude of oscillations. **e**, **f**, Examples of negative control experiments. **e**, Cells containing the repressilator were disrupted by growth in media containing 50 μM IPTG. **f**, Cells containing only the reporter plasmid.

Box 1

Network design

Design of the repressilator started with a simple mathematical model of transcriptional regulation. We did not set out to describe precisely the behaviour of the system, as not enough is known abut the molecular interactions inside the cell to make such a description realistic. Instead, we hoped to identify possible classes of dynamic behaviour and determine which experimental parameters should be adjusted to obtain sustained oscillations.

Deterministic, continuous approximation

Three repressor-protein concentrations, p_i, and their corresponding mRNA concentrations, m_i (where i is *lacI*, *tetR* or *cI*) were treated as continuous dynamical variables. Each of these six molecular species participates in transcription, translation and degradation reactions. Here we consider only the symmetrical case in which all three repressors are identical except for their DNA-binding specificities. The kinetics of the system are determined by six coupled first-order differential equations:

$$\frac{dm_i}{dt} = -m_i + \frac{\alpha}{(1+p_j^n)} + \alpha_0 \qquad \begin{pmatrix} i = lacI, tetR, cI \\ j = cI, lacI, tetR \end{pmatrix}$$

$$\frac{dp_i}{dt} = -\beta(p_i - m_i)$$

where the number of protein copies per cell produced from a given promoter type during continuous growth is α_0 in the presence of saturating amounts of repressor (owing to the 'leakiness' of the promoter), and $\alpha + \alpha_0$ in its absence; β denotes the ratio of the protein decay rate to the mRNA decay rate; and n is a Hill coefficient. Time is rescaled in units of the mRNA lifetime; protein concentrations are written in units of K_M, the number of repressors necessary to half-maximally repress a promoter; and mRNA concentrations are rescaled by their translation efficiency, the average number of proteins produced per mRNA molecule. The numerical solution of the model shown in Fig. 1c used the following parameter values: promoter strength, 5×10^{-4} (repressed) to 0.5 (fully induced) transcripts per s; average translation efficiency, 20 proteins per transcript, Hill coefficient, $n = 2$; protein half-life, 10 min; mRNA half-life, 2 min; K_M, 40 monomers per cell.

This system of equations has a unique steady state, which becomes unstable when $\frac{(\beta+1)^2}{\beta}\frac{\alpha}{} < \frac{3X^2}{4+2X}$, where $X \equiv -\frac{\alpha n p^{n-1}}{(1+p^n)^2}$ and p is the solution to $p = \frac{\alpha}{1+p^n} + \alpha_0$. The boundary between the stable and unstable domains can therefore be plotted (Fig. 1b). The unstable domain becomes much larger when the Hill coefficient increases, removing any limitation on β for sufficiently large α (compare curve B, for which $n = 2$, to curve A, for which $n = 2.1$). The effect of leakiness, α_0, can be seen by plotting the stability boundary for a constant ratio of α_0/α, as in curve C. When α_0 becomes comparable to K_M (1 in our units), the unstable domain shrinks (compare curve B, for which $\alpha_0 = 0$, to curve C, for which $\alpha_0/\alpha = 10^{-3}$). Similar analysis of the stability of the steady state can be performed for generalized models of cyclic transcriptional feedback loops. The simplest such networks supporting limit-cycle oscillations are those containing a single repressor and a single activator, or an odd number of repressors exceeding 3. In general, the period of oscillations in such networks is determined mainly by the protein stability[16]. More detailed calculations, with non-Hill-function repression curves, or using thermodynamic binding energies to predict equilibrium operator occupancies, and taking repressor dimerization into account, yield similar stability results[19]. It is possible that, in addition to simple oscillations, this and more realistic models may exhibit other complex types of dynamic behaviour.

Stochastic, discrete approximation

The preceding analysis neglects the discrete nature of the molecular components and the stochastic character of their interactions, however. Such effects are believed to be important in biochemical and genetic networks[12]. We therefore adapted the above equations to perform stochastic simulations, as described[20]. To obtain cooperativity in repression analogous to the continuous case, we assumed the presence of two operator sites on each promoter and the following reactions: binding of proteins to each operator site (1 $nM^{-1}\,s^{-1}$); unbinding of protein from the first-occupied (224 s^{-1}) and the second-occupied (9 s^{-1}) operator; transcription from occupied ($5 \times 10^{-4}\,s^{-1}$) and from unoccupied (0.5 s^{-1}) promoters; translation (0.167 $mRNA^{-1}\,s^{-1}$); protein decay (10 min half-life); and mRNA decay (2 min half-life). These parameters were chosen to correspond as closely as possible to the continuous model described above, assuming that 1 molecule per cell corresponds to a concentration of ~1 nM. Oscillations persist for these parameter values (Fig. 1c) but with a large variability, resulting in a finite autocorrelation time (compare insets in Fig. 1c).

the noisy repressilator dynamics. In addition, varying the host species and genetic background would allow us to check for, and minimize, spurious interactions with endogenous cellular subsystems, and to investigate how the network is embedded in the cell. For instance, in the repressilator network, the cell-division cycle does not seem to be coupled with the repressilator, as the timing of oscillations is uncorrelated with cell septation events (Fig. 2). However, entry into the stationary phase causes the repressilator to halt, indicating that the network is coupled to the global regulation of cell growth.

The levels of many cellular components vary over time in growing cells, and even strains that constitutively express GFP exhibit significant heterogeneity, so we performed several control experiments to check that the observed oscillations are indeed due to the repressilator (Fig. 3e, f). These included deliberate disruption of the network (by adding sufficient IPTG to interfere with LacI) and observation of GFP expression in the absence of the repressilator (from plasmids with different promoters and origins of replication).

Our results show that it is possible to design and construct an artificial genetic network with new functional properties from generic components that naturally occur in other contexts. Such work is analogous to the rational design of functional proteins from well-characterized motifs[13]. Further characterization of components and alteration of network connectivity may reveal general features of this and related networks, and provide a basis for improved design and possible use in biotechnological applications. Moreover, comparing designed networks with their evolved counterparts may also help us to understand the 'design principles' underlying the latter. For instance, circadian clocks are found in many organisms, including cyanobacteria in which the cell-division time may be shorter than the period[14–15]. However, the reliable performance of such circadian oscillators can be contrasted with the noisy, variable behaviour of the repressilator. Instead of three repressors, it seems that circadian oscillators use both positive and negative control elements. Does this design lead to improved reliability? Recent theoretical analysis suggests that, in the presence of interactions between positive and negative control elements that lead to bistable, hysteretic behaviour, an oscillating circuit does indeed exhibit high noise-resistance[16]. It would be interesting to see whether one could build an artificial analogue of the circadian clock, and, if so, whether such an analogue would display the noise resistance and temperature compensation of its natural counterpart. □

Methods

Network construction

The three repressors (*lacI*, *tetR* and *cI*), the λ promoter P_R and the unstable variants of *gfp*[11] were all cloned by the polymerase chain reaction (PCR) and verified by sequencing. In the case of *lacI*, the GTG start codon was changed to ATG with the 5′ primer. 3′ PCR primers were used to add the coding sequence for the 11-amino-acid *ssrA* tag to the three repressors[8]. Tagging of full-length λ repressor, as well as *lacI* and *tetR*, resulted in functional proteins that required increased induction to achieve full repression, consistent with decreased stability. Promoter sequences $P_L$lacO1 and $P_L$tetO1 were obtained from pZE21-MCSI and pZE12-luc[6]. The repressilator plasmid was constructed in three successive cloning steps from intermediate plasmids containing the three transcriptional units. The reporter plasmid was constructed by cloning the GFPaav variant[11], which has a half-life of around 90 min, into pZE21-MCS1 (ref. 6). The finite rate at which GFP is oxidized to its fluorescent form[17] and its relatively long half-life limit our ability to observe fast dynamic phenomena. The presence of additional *tet* operators on the reporter plasmid constitutes a perturbation to the single-plasmid repressilator network by titrating out repressors[18].

Data acquisition and analysis

Cells of *E. coli lac*$^-$ strain MC4100 (unless otherwise specified) transformed with appropriate plasmids were grown in minimal media (7.6 mM $[NH_4]_2SO_4$, 2 mM $MgSO_4$, 30 μM $FeSO_4$, 1 mM EDTA, 60 mM potassium phosphate, pH 6.8) supplemented with 0.5% glycerol, 0.1% casamino acids and appropriate antibiotics (20 μg ml^{-1} kanamycin or 20 μg ml^{-1} ampicillin), when needed. Time-lapse microscopy was conducted on a Zeiss Axiovert 135TV microscope equipped with a 512 × 512-pixel cooled CCD camera (Princeton Instruments). Cultures were grown for at least 10 hours to optical density of 0.1 at 600 nm, diluted into fresh media, spotted between a coverslip and 1 ml of liquid 2% SeaPlaque low-melt agarose (FMC) in media, and sealed. The temperature of the samples was maintained at 30–32 °C by using Peltier devices (Melcor). Bright-field (0.1 s) and epifluorescence (0.05–0.5 s) exposures were taken periodically (every 5 or 10 min). All light sources (standard 100 W Hg and halogen lamps) were shuttered between exposures. Images were flat-field corrected with custom software. For the synchronization experiment, overnight cultures were diluted back 1:100 in media containing 100 μM IPTG, grown to mid-log, washed several times, and diluted again and grown in 96-well plates at 30 with shaking in a Wallac Victor 2 plate reader, while fluorescence and absorbance measurements were taken every 5 min.

For analysis, cells were selected from the final frames of bright-field movies, without regard to their fluorescence signals, and tracked manually backward in time until the first frame. At each time point, the cell position was identified on the bright-field image, and fluorescence intensity data were averaged over a 28-pixel region, similar in size to the cell diameter, in the corresponding location on the fluorescence image. A fast Fourier transform was applied to the temporal fluorescence signal from each analysed cell lineage and divided by the transform of a decaying exponential with a time constant of 90 min, the measured lifetime of GFPaav. Power spectra exhibiting peaks of more than four times the background at frequencies of 0.2–0.5 per hour were classified as oscillatory (the choice of threshold alters the fraction of oscillatory cells defined by this criterion). The sibling 'decorrelation' half-time was defined as the time necessary for the quantity $|I_1(t) - I_2(t)|/(I_1(t) + I_2(t))$, averaged over pairs of daughter cells, to reach half of its asymptotic value. Here, $I_1(t)$ and $I_2(t)$ denote the fluorescence intensities of the two sibling cells at times, t, starting from the moment of septation (±10 min). In this analysis, only cells judged to be oscillatory by the Fourier criterion were considered.

Various negative control experiments were performed. First, 50 μM IPTG was added to the media to disrupt the functioning of the network (Fig. 3e). Second, we used a version of the repressilator plasmid lacking all but the *tetR* transcriptional unit (in *lacI*^{q} strain JM109). We thus varied GFP expression of the reporter plasmid by controlling TetR levels with 0–20 μM IPTG. Third, we examined cells containing only the reporter plasmid (Fig. 3f). Fourth, we measured GFP expression from reporter plasmids modified in several ways either by replacing the $P_L$tetO1 promoter with each of the two other promoters, and *gfp-aav* with *gfp-lite*[11] (the suffix '*lite*' indicates the presence of a C-terminal *ssrA* tag), or by replacing the ColE1 origin of replication with the lower-copy pSC101 origin normally used on the repressilator plasmid. In none of these control experiments did we observe oscillations similar to those produced by the repressilator.

Received 6 July; accepted 9 November 1999.

1. Bray, D. Protein moelcules as computational elements in living cells. *Nature* **376,** 307–312 (1995).
2. Koshland, D. E. Jr The era of pathway quantification. *Science* **280,** 852–853 (1998).
3. Winfree, A. T. *The Geometry of Biological Time* (Springer, Berlin, 1990).
4. Goldbeter, A. *Biochemical Oscillations and Cellular Rhythms* (Cambridge Univ. Press, 1996).
5. Thomas, R. & D'Ari, R. *Biological Feedback* (CRC Press, Boca Raton, 1990).
6. Lutz, R. & Bujard, H. Independent and tight regulation of transcriptional units in *Escherichia coli* via the LacR/O, the TetR/O and AraC/I1-I2 regulatory elements. *Nucleic Acids Res.* **25,** 1203–1210 (1997).
7. Kushner, S. R. in *Escherichia Coli and Salmonella: Cellular and Molecular Biology* (ed. Neidhardt, F. C.) (ASM, Washington DC, 1996).
8. Keiler, K. C., Waller, P. R. & Sauer, R. T. Role of a peptide tagging system in degradation of proteins synthesized from damaged messenger RNA. *Science* **271,** 990–993 (1996).
9. Gottesman, S., Roche, E., Zhou, Y. & Sauer, R. T. The ClpXP and ClpAP proteases degrade proteins with carboxy-terminal peptide tails added by the SsrA-tagging system. *Genes Dev.* **12,** 1338–1347 (1998).
10. Herman, C., Thevenet, D., Bouloc, P., Walker, G. C. & D'Ari, R. Degradation of carboxy-terminal-tagged cytoplasmic proteins by the *Escherichia coli* protease HflB (FtsH). *Genes Dev.* **12,** 1348–1355 (1998).
11. Andersen, J. B. *et al.* New unstable variants of green fluorescent protein for studies of transient gene expression in bacteria. *Appl. Environ. Microbiol.* **64,** 2240–2246 (1998).
12. McAdams, H. H. & Arkin, A. It's a noisy business! Genetic regulation at the nanomolar scale. *Trends Genet.* **15,** 65–69 (1999).
13. Bryson, J. W. *et al.* Protein design: a hierarchic approach. *Science* **270**, 935–941 (1995).
14. Dunlap, J. C. Molecular bases for circadian clocks. *Cell* **96,** 271–290 (1999).
15. Kondo, T. *et al.* Circadian rhythms in rapidly dividing cyanobacteria. *Science* **275**, 224–227 (1997).
16. Barkai, N. & Leibler, S. Circadian clocks limited by noise. *Nature* (submitted????). **(Eds to update)**
17. Tsien, R. Y. The green fluorescent protein. *Annu. Rev. Biochem.* **67,** 509–544 (1998).
18. Glascock, C. B. & Weickert, M. J. Using chromosomal lacIQ1 to control expression of genes on high-copy-number plasmids in *Escherichia coli*. *Gene* **223,** 221–231 (1998).
19. Elowitz, M. B. *Transport, Assembly, and Dynamics in Systems of Interacting Proteins.* Thesis, Princeton Univ., Princeton (1999).
20. Gillespie, D. T. Exact stochastic simulation of coupled chemical reactions. *J. Phys. Chem.* **81,** 2340–2361 (1977).

Acknowledgements

We thank H. Bujard, S. Freundlieb, A. Hochschild, R. Lutz and C. Sternberg for plasmids and advice; U. Alon, N. Barkai, P. Cluzel, L. Frisen, C. Guet, T. Hyman, R. Kishony, A. Jaedicke, P. Lopez, F. Nédélec, S. Pichler, R. Kishony, T. Silhavy, T. Surrey, J. Vilar, C. Wiggins and E. Winfree for discussions; M. Surette for advice and encouragement; L. Hartwell and C. Weitz for comments on the manuscript; and F. Kafatos and E. Karsenti for hospitality and support at the European Molecular Biology Laboratory (EMBL), where part of this work was done. This work was partly supported by the US National Institutes of Health and the von Humboldt Foundation.

Correspondence and requests for materials should be addressed to M.B.E. (e-mail: melowitz@princeton.edu).